AIP | Journal of Applied Physics

Geometrical scaling law for laser shock processing

Xianqian Wu, Qingming Tan, and Chenguang Huang

Citation: J. Appl. Phys. **114**, 043105 (2013); doi: 10.1063/1.4816487
View online: http://dx.doi.org/10.1063/1.4816487
View Table of Contents: http://jap.aip.org/resource/1/JAPIAU/v114/i4
Published by the AIP Publishing LLC.

Geometrical scaling law for laser shock processing

Xianqian Wu,[1,2] Qingming Tan,[1] and Chenguang Huang[1,a)]
[1]*Key Laboratory of Mechanics in Fluid Solid Coupling Systems, Institute of Mechanics, Chinese Academy of Sciences, Beijing 100190, People's Republic of China*
[2]*Mechanical and Aerospace Engineering, Case Western Reserve University, Cleveland, Ohio 44106, USA*

(Received 6 May 2013; accepted 8 July 2013; published online 25 July 2013)

Scaling approach to laser shock processing is studied by dimensional analysis and numerical simulation. The essential dimensionless parameters controlling the shock effect are studied, and a geometrical scaling law correlating the input laser parameters and the output strengthening effect parameters is presented. The numerical results show that there is a competition controlling mechanism between thickness of confined overlay and laser duration for the surface residual stress; the plastically affected depth increases linearly with increasing laser duration, increases quadratically with increasing laser power density, and is almost independent with the thickness of confined overlay. Based on the results, a window of the optimal working parameters is presented. [http://dx.doi.org/10.1063/1.4816487]

I. INTRODUCTION

Laser shock processing (LSP), which is an advanced surface enhancement technique for metals,[1–4] has been widely adopted in aerospace and automobile industries to improve mechanical behavior of some key components.[5–9] In a typical LSP process, followed by high power density laser irradiating an opaque absorption layer glued on the metallic target surface through a sheet of transparent overlay, a thin surface layer of the metallic target is heated and transformed into plasma state with high electron density and constrained between the transparent overlay and the rest part of the target. Generally, the plasma pressure reaches up to several GPa in tens of nanoseconds. After the laser switches off, the plasma pressure drops sharply according to the rapid adiabatic expansion.[3,10–13] Accompanied with the propagation of the shock pressure, plastic deformation occurs in a surface layer of the metallic material and leaves certain residual stress distribution throughout the plastically affected region.[14,15] Here, we define the depth of the plastically affected region as the distance from the point, where residual stress changes sign from negative to positive, to the free surface. The magnitude of the depth of plastically affected region and the residual stress are important for evaluating the shock effects of LSP. The characteristic parameters describing the residual stress distribution include the residual stress at the surface of the plastically affected region σ_{surf}, the plastically affected depth L_p, etc.

However, it is difficult to achieve optimized parameters by theoretical analysis because LSP is a complex process influenced by multiple parameters such as laser parameters (e.g., laser power density, laser spot size, and shape) and material parameters (e.g., mechanical and thermo-dynamical properties of confined overlay, absorption layer, and metallic target). Ballard[14] derived the relationships between shock effects and shock pressure applied on the surface of metallic target. In his analysis, the pressure is assumed as uniform in spatial and triangular in temporal. In addition, the elastic-perfectly plastic behavior of target was taken into account. Recently, Wu and Shin[16] analyzed the residual stress distribution under given laser parameters by a physical model. The shock relation was taken into account, and the inertial confinement effects of the transparent overlay and the metallic target were not concerned with. The most related studies on LSP focused attention on experiments to obtain the influence of individual parameter such as laser spot shape and its intensity, or mechanical properties of confined overlay, etc.[5,14,17–23] However, essential dimensionless parameters, which determine the characteristics of residual stress distribution, have not been shed light on the mechanism clearly yet.

In response to the deficiency of the related issues mentioned above, the present paper focuses attention on the analysis of the dimensionless cause and effect relationship for LSP. Meanwhile, the effects of bulk compressibility and inertial confinement of confined overlay and metallic target are examined in the present analysis. This paper is organized as follows. In Sec. II, the essential dimensionless parameters in LSP are deduced by dimensional analysis. Especially, a geometrical scaling law is derived. In Sec. III, a numerical simulation scheme for LSP is given, in which the effects of bulk compressibility and inertial confinement of confined overlay and metallic target are taken into account. In Sec. IV, the numerical results are given and discussed. The geometrical scaling law is validated, and the influence of dimensionless parameters on shock effects is analyzed.

II. DIMENSIONAL ANALYSIS OF LSP

For the sake of simplicity, some assumptions are made as follows. The materials of the absorption layer and the target are the same metallic material. High power density laser deposits in a thin layer of metallic target surface in a short time. The deposited energy is used to melt, vaporize, and ionize a thin surface layer of the metallic target, and then such layer is transformed into a plasma layer with high temperature and high pressure instantaneously. The thin layer of plasma continues to absorb the laser energy through inverse

a)Electronic mail: huangcg@imech.ac.cn1

bremsstrahlung absorption mechanism until the laser light source switches off.[3] The laser absorption coefficient of the metallic target is assumed as A. After the laser switches off, the heated plasma layer expands adiabatically.

As the plasma is constrained between the confined overlay and target all the time, a shock wave propagates deeper into the target to induce plastically toughening effect. The mechanical behavior of the target is improved eventually because of the effects of bulk compressibility and inertial confinement of confined overlay and metallic target. The Mie-Grüneisen equation of state (EOS) is adopted to describe the bulk compressive behavior,

$$p - p_k(V) = \gamma/V \cdot [E - E_k(V)], \tag{1}$$

where p, V, and E are pressure, specific volume, and internal energy, respectively; γ is Mie-Grüneisen coefficient; $p_k(V)$ and $E_k(V)$ are pressure and specific internal energy at 0 K, respectively. Because the relationship between the pressure $p_H(V)$ and specific internal energy $E_H(V)$ along the Hugoniot line can be measured by shock experiments, Eq. (1) can be replaced by the following equation:[24,25]

$$p - p_H(V) = \gamma/V \cdot [E - E_H(V)]. \tag{2}$$

Additionally, $p_H(V)$ and $E_H(V)$ can be determined with the relationship between shock velocity U and particle velocity u, which satisfies an empirical linear expression,

$$U = c + b \cdot u, \tag{3}$$

where c and b are material constants. To consider the inertial confinement, the thickness of the confined overlay and the metallic target is taken into account.

Based on the physical description, dimensional analysis method is taken to analyze the glass-confined LSP process. Note that water-confined LSP is more popular in practice. However, glass-confined LSP experiments could be easily controlled and repeatable. Nevertheless, we think that, the similar analysis could be performed if taking a layer of water as confinement by using the parameters of water instead of BK7 glass. Through appropriate dimensionless analysis, causality of physical phenomena can be highlighted.[26] The parameters controlling the effect of LSP are described in Fig. 1 and listed as follows:

High power density laser: rate of energy flow J, laser duration (full width at half maximum, FWHM) τ, and spot area S.

Laser absorption coefficient of metallic target: A.

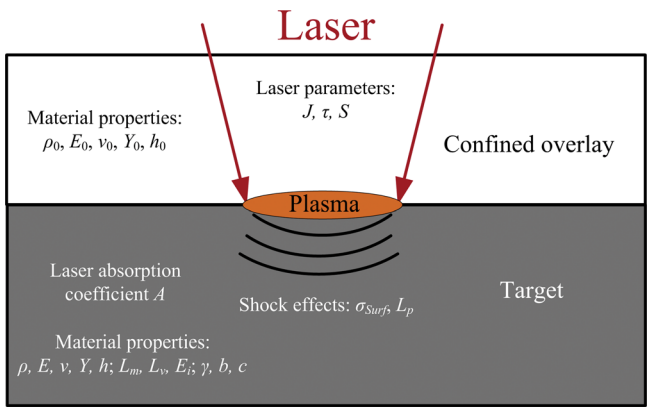

FIG. 1. Parameters of laser, confined overlay, and metallic target in glass-confined LSP regime. The material of the absorption layer is same as the target to simplify the analysis.

Confined overlay: initial density ρ_0, Young's modulus E_0, Poisson's ratio ν_0, yield stress Y_0, and thickness h_0.

Metallic target: initial density ρ, Young's modulus E, Poisson's ratio ν, yield stress Y, thickness h; latent heat of fusion L_m, latent heat of vaporization L_ν, and ionization energy E_i; Mie-Grüneisen EOS coefficient γ, b, and c, where the metallic target is assumed to be described by hydro-elastoplastic model.[27] Such constitutive model consists of volumetric change part and shape distortion part. The volumetric change part satisfies Mie-Grüneisen EOS and the shape distortion part satisfies elasto-perfectly plastic relationship between deviatoric stress and deviatoric strain.

The eventual shock effects on metallic target, characterized by the surface residual stress at the center of the impact region, σ_{surf}, and the depth of the plastically affected depth along the central axis of the impact region, L_p, should be a function of the governing parameters characterizing the laser, the confined overlay, and the metallic target,

$$\sigma_{surf} = f(AJ, \tau, S; \rho_0, E_0, \nu_0, Y_0, h_0; \rho, E, \nu, Y, L_m, L_\nu, E_i, \gamma, b, c, h), \tag{4}$$

$$L_p = g(AJ, \tau, S; \rho_0, E_0, \nu_0, Y_0, h_0; \rho, E, \nu, Y, L_m, L_\nu, E_i, \gamma, b, c, h). \tag{5}$$

Generally, in LSP the thickness of metallic target, h, is relatively large enough, and thereby the metallic target can be approximately considered as infinitely thick. While considering the effect of parameter h, a similar analysis could be performed. Taking laser spot area S, initial density ρ, and Mie-Grüneisen parameter c of metallic target as a unit system, the following dimensionless relationships can be obtained:

$$\frac{\sigma_{surf}}{Y} = f\left(\frac{AJ}{\rho c^3}, \frac{\tau}{S^{1/2}/c}; \frac{\rho_0}{\rho}, \frac{E_0}{E}, \frac{Y_0}{Y}, \frac{h_0}{S^{1/2}}, \nu_0; \frac{Y}{E}, \frac{\rho\nu^2/Y}{M^2}, \frac{L_m}{c^2}, \frac{L_\nu}{c^2}, \frac{E_i}{c^2}, \gamma, b, \nu\right), \tag{6a}$$

$$\frac{L_p}{S^{1/2}} = g\left(\frac{AJ}{\rho c^3}, \frac{\tau}{S^{1/2}/c}; \frac{\rho_0}{\rho}, \frac{E_0}{E}, \frac{Y_0}{Y}, \frac{h_0}{S^{1/2}}, \nu_0; \frac{Y}{E}, \frac{\rho\nu^2/Y}{M^2}, \frac{L_m}{c^2}, \frac{L_\nu}{c^2}, \frac{E_i}{c^2}, \gamma, b, \nu\right), \tag{6b}$$

where $M = \nu/c$ is Mach number. The physical meanings of the dimensionless parameters are as follows:

$\frac{AJ}{\rho c^3}$: represents the ratio of energy deposition effect to compressible effect of the target.
$\frac{\tau}{S^{1/2}/c}$: represents the ratio of loading duration to unloading duration in the target.
$\frac{\rho_0}{\rho}, \frac{E_0}{E}, \frac{Y_0}{Y}$: represent the characteristic density, elastic modulus, and yield stress of the confined overlay, respectively.
$\frac{h_0}{S^{1/2}}$: represents the ratio of inertial confinement effect to the unloading effect from the free surface.
$\frac{Y}{E}$: represents the elastic deformation limit of the target.
$\frac{\rho\nu^2/Y}{M^2}$: represents ratio of Cheng constant[27] to Mach number.
$\frac{L_m}{c^2}, \frac{L_v}{c^2}, \frac{E_i}{c^2}$: represent the ratios of fusion effect, vaporization effect, and ionization effect to compressible effect of the target, respectively.
γ, b: are adiabatic exponent and constant of Hugoniot equation of state of the target, respectively.
ν_0, ν: are Poisson's ratios of confined overlay and target, respectively.

The 12 material related dimensionless parameters in the bracket on the right hand side in Eqs. (6a) and (6b) remain constant, if the parameters of confined overlay and metallic target are unchanged. Therefore, simpler relationships are achieved as follows:

$$\frac{\sigma_{surf}}{Y} = f\left(\frac{AJ}{\rho c^3}, \frac{\tau}{S^{1/2}/c}, \frac{h_0}{S^{1/2}}\right), \tag{7a}$$

$$\frac{L_p}{S^{1/2}} = g\left(\frac{AJ}{\rho c^3}, \frac{\tau}{S^{1/2}/c}, \frac{h_0}{S^{1/2}}\right). \tag{7b}$$

It is obvious that a geometrical scaling law holds for LSP process. For the maximum residual stress, σ_{max}, and its located depth, L_{max}, the geometrical scaling law can also be deduced in the same way,

$$\frac{\sigma_{max}}{Y} = \tilde{f}\left(\frac{AJ}{\rho c^3}, \frac{\tau}{S^{1/2}/c}, \frac{h_0}{S^{1/2}}\right), \tag{7c}$$

$$\frac{L_{max}}{S^{1/2}} = \tilde{g}\left(\frac{AJ}{\rho c^3}, \frac{\tau}{S^{1/2}/c}, \frac{h_0}{S^{1/2}}\right). \tag{7d}$$

From Eqs. (7a) to (7d), the same distribution of residual stress will be left in the target, while the dimensionless parameters $AJ/\rho c_3$, $\tau_p/(S^{1/2}/c)$, and $h_0/S^{1/2}$ are unchanged in LSP.

III. NUMERICAL SIMULATION

Based on coupling behavior between the laser induced plasma evolution and the dynamic deformation of the confined overlay and the metallic target, numerical simulation is implemented to validate the geometrical scaling law and to understand the influence of dimensionless parameters on toughening effects. With the high power density laser irradiating the metallic target surface through the transparent overlay, laser energy deposits in a thin surface layer of metallic target, and the phase of the latter changes from solid one into plasma one with high pressure and high temperature simultaneously. After the laser switches off, the plasma expands adiabatically. In the whole LSP process, the laser induced plasma is constrained between the confined overlay and the metallic target by the bulk compressibility and inertial confinement, which induces the shock effects such as surface residual stress, σ_{surf}, and the depth of plastically deformed region, L_p, in the metallic target eventually.

As shown in Fig. 2, after a beam of laser with certain wavelength and power density $J(t)$ irradiates the surface of metallic target through the transparent confined overlay, the laser energy deposits in a thin surface layer of the metallic target in a short time with a depositing rate $AJ(t)$, where A is the absorption coefficient of the metallic target as mentioned in Sec. II. The deposited energy is used for melting, vaporization, and ionization, for which the characteristic parameters are the target's latent heat of fusion L_m, latent heat of vaporization L_v, and ionization energy E_i, respectively. The phase transition of the confined overlay is not taken into account because of its negligible absorption coefficient. Denote the laser ablation velocity of the metallic surface as $u_{T,ev}(t)$, and the thickness and the pressure of the plasma as $L(t)$ and $p(t)$, respectively. Meanwhile, the plasma continues to absorb the irradiating laser energy through inverse bremsstrahlung absorption mechanism until the laser switches off, by which the internal energy $e(t)$ and pressure $p(t)$ of the plasma increase quickly. The internal energy of the plasma is composed of the ionization energy $e_i(t)$ and thermal energy $e_T(t)$. The laser power density absorbed by the plasma is $J_P(t) = AJ(t)[1 - \exp(-\kappa_p L(t))]$, where κ_p is the absorption coefficient of plasma. We assumed that the fraction of laser power density, $J_T(t) = AJ(t)\exp(-\kappa_p L(t))$, is deposited and absorbed by a thin surface layer of the metallic target, and the absorbed energy is transferred to internal energy and the work against to the neighboring overlay and the metallic part. After the laser switches off, the plasma, confined between the confined overlay and metallic target, expands adiabatically, and the shock effects on the metallic target are left eventually. At the same time, the confined overlay and the undisturbed metallic target are deformed under the plasma pressure $p(t)$, which induces moving velocities at the interfaces between the thin plasma layer and its neighbors, the confined overlay, and the undisturbed metal part. The moving velocities are denoted as $u_C(t)$ and $u_T(t)$, respectively. As depicted in Fig. 2, the reference frames Or_1 and Or_2 are taken for the deformation of the confined overlay and the undisturbed part, respectively. The increasing rate of the thickness of plasma is then determined by the interface moving velocities of the confined overlay and the undisturbed metallic part.

A. Mathematical formulation of plasma evolution

With laser irradiating the metallic target energy conservation governs the plasma evolution, in which the deposited laser energy absorbed by plasma is transferred to the internal energy e of the plasma and the external work W against to the plasma boundaries,

$$AJ(\mathrm{t})\mathrm{d}t = \mathrm{d}W + \mathrm{d}e, \tag{8}$$

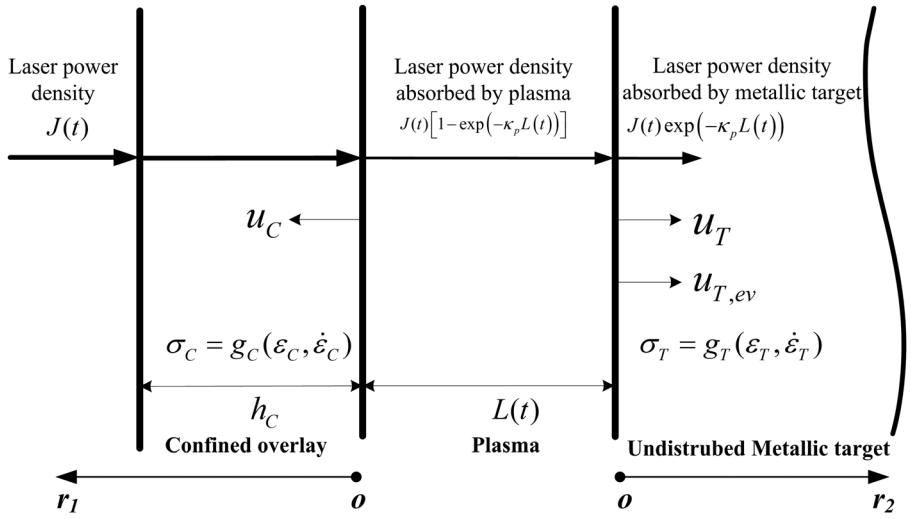

FIG. 2. Sketch of the numerical model. The model places emphasis on the coupling effect between plasma expansion and dynamic behavior of materials. The inertial confinement of the confined overlay is illuminated, which is represented by the thickness of confined overlay.

where

$$dW = p(t) \cdot dL(t), \tag{9}$$

$p(t)$ is the average pressure in the plasma and $L(t)$ is the thickness of the plasma.

Refer to Fabbro *et al.*,[3] we assume that a fraction α of internal energy of plasma is thermal energy $e_T(t)$ and another fraction $1-\alpha$ is the energy used to ionize the high temperature gas to form the plasma,

$$\alpha = e_T(t)/e(t). \tag{10}$$

Assume α is constant in the laser-plasma interaction and typically take as 0.1 in the simulation. Additionally, as Fabbro *et al.*,[3] supposing the thermal energy of the plasma is related with pressure $p(t)$ and thickness $L(t)$ of the plasma, then

$$e_T(t) = \frac{3}{2}[p(t)L(t)]. \tag{11}$$

Accordingly, Eq. (8) can be rewritten as

$$AJ(t) = p(t)\frac{dL(t)}{dt} + \frac{3}{2\alpha}\frac{d[p(t)\times L(t)]}{dt}. \tag{12}$$

When the laser light source switches off, the plasma expands adiabatically,

$$p(t) = p(\tau)\left(\frac{L(\tau)}{L(t)}\right)^{\gamma}, \tag{13}$$

where γ is the adiabatic exponent and typically taken as 2.0, and $p(\tau)$ and $L(\tau)$ are the pressure and thickness of the plasma at the time that laser light source switches off, respectively.

The initial conditions are

$$L(0) = 0; \quad p(0) = 0. \tag{14}$$

The boundary conditions are

$$dL(t)/dt = u_C(t) + u_T(t) + u_{T,ev}(t), \tag{15}$$

where $u_{T,ev}(t)$ is the propagation velocity of the laser ablation front, i.e.,

$$u_{T,ev} = \begin{cases} \dfrac{J_T(t)}{\rho(L_m + L_\nu + E_i)} = \dfrac{AJ(t)\exp\left(-\kappa_p L(t)\right)}{\rho(L_m + L_\nu + E_i)}, & t \le \tau \\ 0, \textit{otherwise} \end{cases}. \tag{16}$$

B. Mathematical formulation of confined overlay and undisturbed metallic target

In Eq. (15), the velocities $u_C(t)$ and $u_T(t)$ are related with the dynamic behavior of the confined overlay and undisturbed metallic target under plasma pressure $p(t)$, respectively. The following relationships for the confined overlay and undisturbed metallic target are based on Hamiltonian variational principle,

$$\int_V \rho_C \ddot{U}_C(t)\delta U_C(t)dV + \int_V \sigma_C(t)\delta U_C(t)dV - \int_S p(t)\delta U_C(t)dS = 0, \tag{17}$$

$$\int_V \rho_T \ddot{U}_T(t)\delta U_T(t)dV + \int_V \sigma_T(t)\delta U_T(t)dV - \int_S p(t)\delta U_T(t)dS = 0, \tag{18}$$

where $U_C(t)$ and $U_T(t)$ are displacements, and $\ddot{U}_C(t)$ and $\ddot{U}_T(t)$ are accelerations of confined overlay and undisturbed metallic target, respectively.

The initial conditions are

$$U_C(t)|_{t=0} = 0, \sigma_C(t)|_{t=0} = 0; \quad U_T(t)|_{t=0} = 0, \sigma_T(t)|_{t=0} = 0. \tag{19}$$

The boundary conditions are

$$\sigma_C(t)|_{r_1=0} = p(t), \sigma_C(t)|_{r_1=h_0} = 0; \\ \sigma_T(t)|_{r_2=0} = p(t), \sigma_T(t)|_{r_2\to+\infty} = 0. \tag{20}$$

From Eqs. (8) to (20), the velocity $u_C(t) = \dot{U}_C(t)$ and $u_T(t) = \dot{U}_T(t)$, as well as the surface stress $\sigma_{surf\_t}(t)$ and the plastically affected depth $L_{p\_t}(t)$ can be solved, where $\dot{U}_C(t)$ and $\dot{U}_T(t)$ are velocity of confined overlay and undisturbed metallic target, respectively. In addition, the final surface residual stress σ_{surf} and the plastically affected depth L_p can be obtained as

$$\sigma_{surf} = \sigma_{surf\_t}(t)|_{t\to\infty}, \tag{21}$$

$$L_p = L_{p\_t}(t)|_{t\to\infty}. \tag{22}$$

C. Numerical simulation method

Based on Eqs. (8) to (22), it could be found that the boundary velocity $u_C(t)$ and $u_T(t)$ as well as the plasma pressure $p(t)$ are determined by the laser energy flow, the thickness of the confined overlay and dynamic behavior of the confined overlay and undisturbed metallic target,

$$u_C(t) = f_C(t, AJ, \tau, S; \rho_0, E_0, \nu_0, Y_0, h_0; \rho, E, \nu, Y; \gamma, b, c), \tag{23}$$

$$u_T(t) = f_T(t, AJ, \tau, S; \rho_0, E_0, \nu_0, Y_0, h_0; \rho, E, \nu, Y; \gamma, b, c), \tag{24}$$

$$p(t) = f_p(t, AJ, \tau, S; \rho_0, E_0, \nu_0, Y_0, h_0; \rho, E, \nu, Y; \gamma, b, c). \tag{25}$$

Because the evolution of the plasma and the dynamical deformation of the confined overlay and the undisturbed metallic target are coupled with each other, Eqs. (8) to (20) should be solved simultaneously. A coupling explicit finite differential code with first order precision is developed,[12] by which the plasma pressure and the surface residual stress, σ_{surf}, and plastically affected depth, L_p, of the metallic target can be calculated. The LS-DYNA explicit package[28] is taken to analyze the dynamic behavior of the confined overlay and the undisturbed metallic target under the pressure $p(t)$. The three-dimensional numerical models for confined overlay and metallic target will be described in detail at the next subsection. Then, the LS-PREPOSTD code is used to obtain the surface velocities $u_C(t)$ and $u_T(t)$ for confined overlay and undisturbed metallic target, respectively. As the laser duration τ is fairly short, the time increment is taken as $\Delta t = \tau/100$ in the simulation when the laser irradiates the target. After that the time increment is taken as $\Delta t = \tau/50$ when the laser switches off. The time increments chosen in the simulation meet the convergent condition $\Delta t \le \Delta l/c_0$, where Δl is the minimum length of elements, c_0 is the sound velocity of materials.

1. Finite element model

As shown in Fig. 3, three-dimensional quarter-symmetric finite element models of confined overlay (Fig. 3(a)) and metallic target (Fig. 3(b)) are developed using LS-DYNA package, in which the dimensionless coordinates $x^* = x/S^{1/2}$, $y^* = y/S^{1/2}$, $z^* = z/S^{1/2}$, and $t^* = t/\tau$ are used. The models represent a square area with unit value of a confined overlay with thickness $h_0/S^{1/2}$ and a metallic target with infinite thickness, respectively, both of which are shocked by the dimensionless plasma pressure $p(t)/(\rho c^2)$ with uniform spatial distribution. The lower boundary of the target is nonreflective boundary condition. The confined overlay and the metallic target are fine meshed.

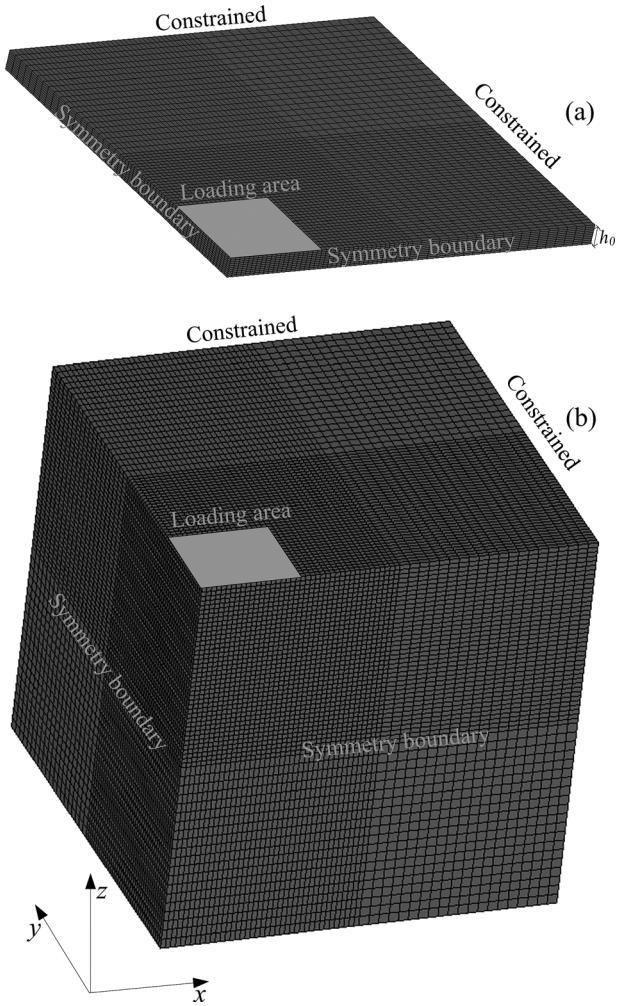

FIG. 3. Three-dimensional quarter-symmetric finite element models for confined overlay and metallic target. The pressure is uniformly applied on the loading squared areas of the confined overlay and metallic target.

In our simulation, BK7 glass and 2024 aluminum alloy are chosen as model materials for confined overlay and metal target, respectively. The elastic-perfect-plastic constitutive model is taken for BK7 glass with initial density $\rho_0 = 2.52 \times 10^3\,\mathrm{kg\cdot m^{-3}}$, Young's modulus $E_0 = 82.3$ GPa, Poisson's ratio $\nu_0 = 0.209$, and yield stress $Y_0 = 1.6$ GPa.[29,30] For 2024 aluminum alloy, the power law constitutive model is taken to describe the plastic flow behavior,[31]

$$\sigma_y = A + B\varepsilon_p^n, \tag{26}$$

where ε_p is equivalent plastic strain, A and B are material constants, and n is the work hardening exponent. The bulk

TABLE I. Mechanical parameters of 2024 aluminum alloy.[31]

ρ (kg/m^3)	E (GPa)	ν	A (MPa)	B (MPa)	n	c (m/s)	b	γ
2.77×10^3	73.8	0.3	265	426	0.34	5.33×10^3	1.34	2.0

compressibility of 2024 aluminum alloy is described by Mie-Grüneisen EOS. Its material properties are given in Table I.

2. Validation of numerical models

The convergence of the numerical simulation results has been validated by comparing with the experimental results of Ref. 13. The simulated residual stresses along $x/S^{1/2}$ direction are shown in Fig. 4, where the minimum length of elements $\zeta^*=0.05$ and the time increment $t^*=0.02$. The simulated results agree well with the experimental results, which validates the convergence of the numerical simulation for $\zeta^*=0.05$ and $t^*=0.02$. Therefore, the same values of ζ^* and t^* are taken in the simulation.

IV. RESULTS AND DISCUSSION

In this section, validation of the geometrical scaling law will be shown, and the numerical results for the influence of dimensionless parameters, including the laser parameters and the metallic target parameters, on the shock effects are analyzed. The material parameters are kept constant in the numerical simulation and listed in Table II. According to the parameters used in LSP technique, the variation ranges of dimensionless thickness of confined overlay, laser pulse duration, and laser power density are chosen as follows:

$$h_0/S^{1/2}\in(0.2,0.1),\ \tau/(S^{1/2}/c)\in(0.02,0.16),\quad AJ/(\rho c^3)\in(0.0125,0.25). \tag{27}$$

First, in order to validate the geometrical scaling law deduced in Sec. II, the shock effects for constant dimensionless thickness and laser duration are numerically simulated, in which three sets of the parameters (τ, $S^{1/2}$, and h_0) are set, i.e., (50.0 ns, 2.5 mm, 0.25 mm), (30.0 ns, 1.5 mm, 0.15 mm), and (20.0 ns, 1.0 mm, 0.10 mm), which have the common reduction ratio (5:3:2). The simulated residual stress distribution in depth of the metallic target is given in Fig. 5. As a squared laser spot is used in the simulation, the surface stress σ_{surf} in the center of impact region is calculated as $\sigma_{surf}=\sqrt{\sigma_x^2+\sigma_y^2}$. The numerical results show that the dimensionless surface residual stresses and plastically affected depths of the metallic target for the three sets of parameters are all about 0.76 and 1.49. The residual stress distributions in depth for the three sets of the parameters are almost the same, which demonstrates that the geometrical scaling law of LSP deduced in Sec. II surely holds. The geometrical scaling law is useful in LSP experiments, because the number of the independent parameters can be reduced and the experimental efficiency can be improved significantly in order to obtain an optimized parameter window.

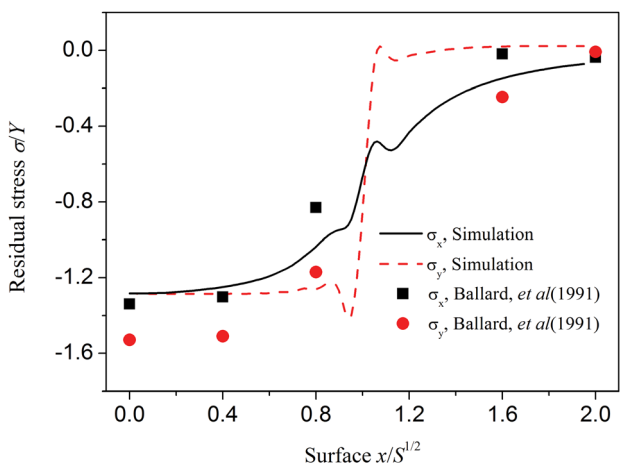

FIG. 4. Residual stresses along $x/S^{1/2}$ of the present simulated results and the experimental measurement of Ballard *et al.* (1991), in which the same pressure and material are used in the simulation. The minimum length of elements $\zeta^*=0.05$ and the time increment $t^*=0.02$ are used in the simulation.

Second, the influence of thickness of confined overlay, laser duration, and laser power density on LSP effects is numerically simulated and analyzed. The variation ranges of dimensionless thickness of confined overlay, laser pulse duration, and laser power density for numerical simulation are given in formula (27), and the related dimensionless material parameters are listed in Table II. The influence of dimensionless thickness of confined overlay and laser duration on dimensionless surface residual stress and plastically affected depth is numerically simulated, and the numerical results are shown in Figs. 6 and 7, in which $AJ/(\rho c^3)=0.033$ and the other dimensionless parameters are kept constant as given in Table II. From Fig. 6, it shows that curved surface of surface residual stress exhibits a similar inclined saddle-typed surface with an obviously peak at the center ($h_0/S^{1/2}=0.10$ and $\tau/(S^{1/2}/c)=0.146$). Denote $a=h_0/S^{1/2}$ and $b=\tau/(S^{1/2}/c)$. Along the intersection curve of the curved surface of surface residual stress and plane $0.14a+b=0.16$, the surface residual stress decreases with increasing the thickness of confined overlay or decreasing the laser duration except the peak value at the center of the surface, which implies that, in terms of the surface residual stress, the shock effect is improved with increasing the thickness of confined overlay and decreasing the laser duration simultaneously. Along the intersection curve of the curved surface of surface residual stress and plane $-0.14a+b=0.02$, the surface residual stress increases with increasing thickness of confined overlay or increasing laser duration if $a<0.5$ and $b<0.09$. Otherwise, the surface residual stress decreases with increasing the thickness of confined overlay or increasing laser duration. In other word, in terms of the surface residual stress, the shock effect is improved with increasing or decreasing the thickness of confined overlay and laser duration simultaneously backwards to the point ($a=0.5$, $b=0.09$). Generally, increasing laser duration will increase pressure duration, which will increase plastically affected depth and increase surface residual stress finally.[10,32] Based on the simulated result as depicted in Fig. 6, the tendency between the laser duration and surface residual stress agrees with the

TABLE II. Material related dimensionless parameters.

$\frac{\rho_0}{\rho}$	$\frac{E_0}{E}$	$\frac{Y_0}{Y}$	$\frac{Y}{E}$	$\frac{\rho v^2/Y}{M^2}$	$\frac{L_m}{c^2}$	$\frac{L_y}{c^2}$	$\frac{E_i}{c^2}$	γ	b	ν_0	ν
0.91	0.90	6.04	3.59×10^{-3}	2.65×10^{2}	3.61×10^{-3}	0.10	0.19	2.0	1.34	0.21	0.30

simulated results, while the dimensionless thickness of confined overlay is smaller than 0.3. After that the tendency is inhibited, indicating the effect of inertial confinement of confined overlay on improving the shock effect. Note that while the thickness of confined overlay exceeds 0.7, a slightly inverse tendency between the surface residual stress and laser duration is exhibited. The influence of thickness of confined overlay and laser duration on the surface residual stress implies that there is a competition mechanism, especially the peak value at the center of the saddle-typed surface may imply a transition of controlling mechanism, which will be further studied in the future by experiments. From Fig. 7, it shows that the curved surface of plastically affected depth also exhibits a similar inclined saddle-typed surface. However, the curvature of the curved surface of plastically affected depth is much small compared with that of the surface residual stress. The plastically affected depth increases almost monotonically with increasing laser duration, which agrees with the experimental results of Fairand and Clauer,[33] Anderholm,[34] and Peyre.[22] In addition, the plastically affected depth is almost independent with the thickness of confined overlay when dimensionless laser duration $\tau/(S^{1/2}/c)$ is less than 0.12. However, when laser duration $\tau/(S^{1/2}/c)$ exceeds 0.12, the plastically affected depth slightly decreases at the beginning and then increases with increasing thickness of confined overlay.

The relationships between dimensionless thickness of confined overlay and dimensionless surface residual stresses and plastically affected depth are depicted as Fig. 8, where $\tau/(S^{1/2}/c) = 0.1066$, and $AJ/(\rho c^3) = 0.033$, and the other dimensionless parameters are the same as that in Table II. The dimensionless surface residual stress decreases exponentially with increasing dimensionless thickness of confined overlay. With increase of thickness of confined overlay, the effect of bulk compressibility and inertial confinement are reinforced, which extends the loading duration and decreases the surface residual tensile stress of the metallic target eventually. In the previous studies, the temporal profile of the pressure is supposed to be triangular shape, which is governed by the peak laser power density and laser duration. However, our simulation shows that the thickness of confined overlay will extend the loading duration and affects the shock effects of the metallic target. A saturation of surface residual stress is exhibited when the dimensionless thickness exceeds 0.6, indicating the saturation of bulk compressibility and inertial confinement of confined overlay. As shown in Fig. 8, the plastically affected depth increases with increasing thickness of confined overlay, also owing to the reinforcement of bulk compressibility and inertial confinement effect for a much thick confined overlay. A saturation of plastically affected depth is attained at $h_0/S^{1/2} = 0.4$. As $h_0/S^{1/2}$ exceeds 0.4, the plastically affected depth approaches to a constant 1.63. Generally, the bulk compressibility of confined overlay was studied in literatures.[33,35] However, our simulation results demonstrate that the inertial confinement of confined overlay greatly affects the shock effects. A much thick confined overlay is benefit for LSP for a certain laser spot size, and there is a critical thickness of confined overlay. Exceeding the critical value the shock effect will be saturated. It will be speculated if the critical thickness of confined overlay is the

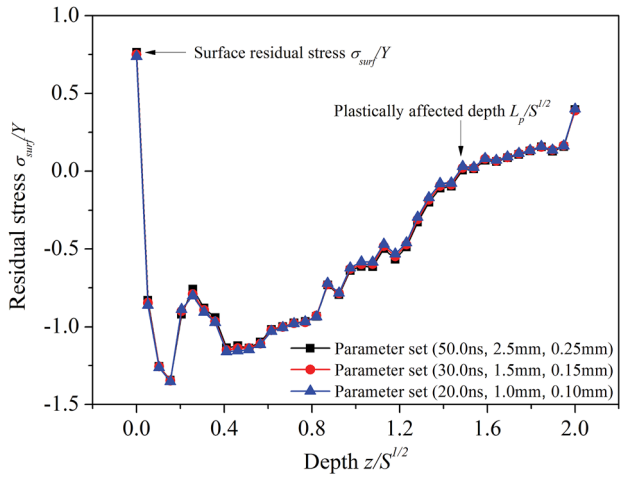

FIG. 5. Residual stress distribution in depth at the center of the impact region for sets of the parameters (τ, $S^{1/2}$, and h_0) are (50.0 ns, 2.5 mm, 0.25 mm), (30.0 ns, 1.5 mm, 0.15 mm), and (20.0 ns, 1.0 mm, 0.10 mm). The other dimensionless parameters are kept constant as given in Table II.

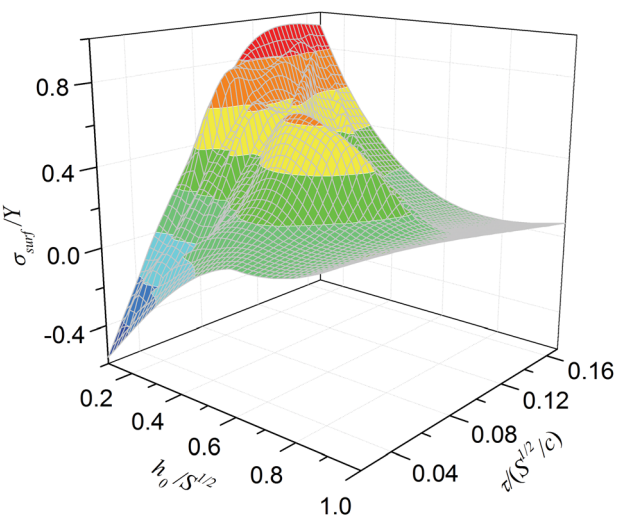

FIG. 6. Influence of laser duration and thickness of confined overlay on surface residual stress of metallic target, in which the dimensionless thickness of confined overlay ranges from 0.2 to 0.1, the dimensionless laser duration ranges from 0.02 to 0.16, and the dimensionless laser power density is fixed as 0.033. The other dimensionless parameters are kept constant as given in Table II. The curved surface obviously exhibits a saddle-typed surface with a peak value at the center of the surface.

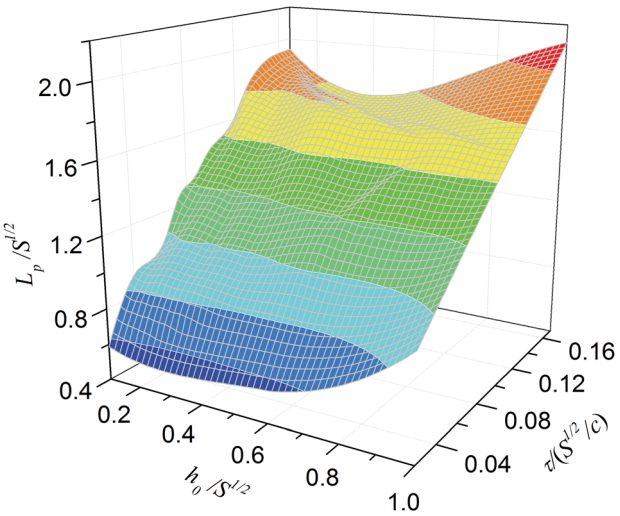

FIG. 7. Influence of laser duration and thickness of confined overlay on plastically affected depth of metallic target, in which the dimensionless thickness of confined overlay ranges from 0.2 to 0.1, the dimensionless laser duration ranges from 0.02 to 0.16, and the dimensionless laser power density is fixed as 0.033. The other dimensionless parameters are kept constant as given in Table II. The curved surface also exhibits saddle-typed surface with much small curvature, and the effect of inertial confinement is slight for plastically affected depth.

same for different material system, which will be investigated in future by strategical LSP experiments.

Moreover, the influence of dimensionless laser duration on the shock effects is simulated and the result is given in Fig. 9, where $h_0/S^{1/2} = 0.1$, $AJ/(\rho c^3) = 0.033$ and the material parameters are kept constant as shown in Table II. From Fig. 9, it shows that the dimensionless plastically affected depth increases linearly with increasing laser duration for given thickness of confined overlay and laser power density, which is consistent with the experimental results of Fairand and Clauer,[33] Anderholm,[34] and Peyre *et al.*,[22] and the theoretical analysis result of Ballard.[14] However, the influence of laser duration on surface residual stress exhibits two stages divided at $\tau/(S^{1/2}/c) = 0.128$. Before this critical value, the surface residual stress increases linearly with increasing laser

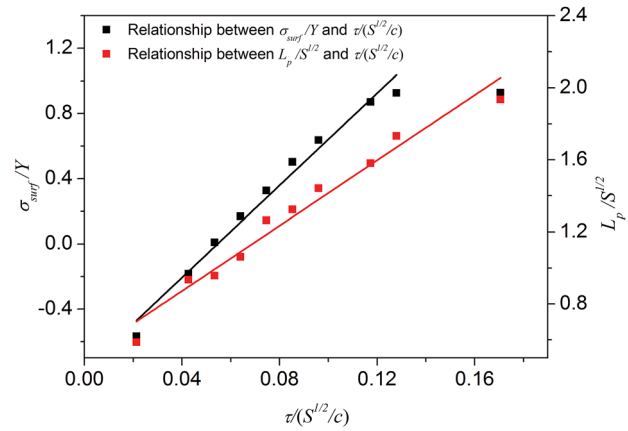

FIG. 9. Influence of laser duration on shock effects, in which the dimensionless thickness of confined overlay and the dimensionless laser power density are fixed as 0.1 and 0.033, respectively, and the dimensionless laser duration ranges from 0.02 to 0.16. The other dimensionless parameters are kept constant as given in Table II.

duration. When the laser duration exceeds the critical value a saturation even decrease of surface residual stress is shown in Fig. 6, which has not been presented in the previous literatures. However, based on the analysis of Ballard,[14] the surface residual stress will increase linearly with increasing laser duration. Note that the critical value of laser duration will decrease with increasing thickness of confined overlay as depicted in Fig. 6. The mechanism of saturation of surface residual stress while laser duration exceeding critical value will be further studied in future. Therefore, the increase of laser duration will lead to deeper plastically affected depth, which is benefit for LSP effects. Meanwhile, the surface residual stress could be improved by increasing thickness of confined overlay for much longer laser duration.

Finally, the influence of laser power density on the shock effects of metallic target is simulated as shown in Fig. 10, in which the dimensionless thickness of confined overlay and laser duration are taken as 0.10 and 0.1066, respectively, and the material parameters are kept constant as given in Table II. From Fig. 10, it shows that the surface residual

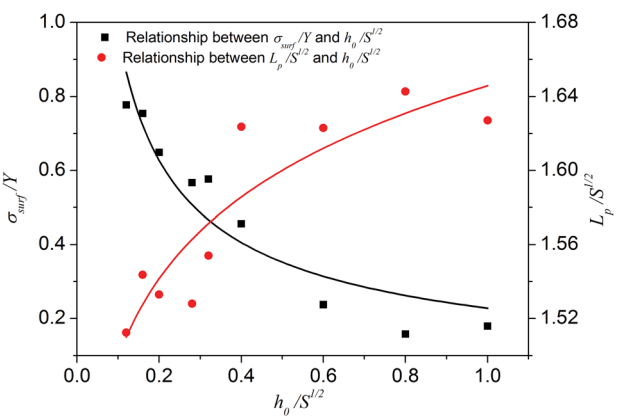

FIG. 8. Influence of thickness of confined overlay on dimensionless shock effects, in which the dimensionless laser duration and the dimensionless laser power density are fixed as 0.1066 and 0.033, respectively, and the dimensionless thickness of confined overlay ranges from 0.2 to 0.1. The other dimensionless parameters are kept constant as given in Table II.

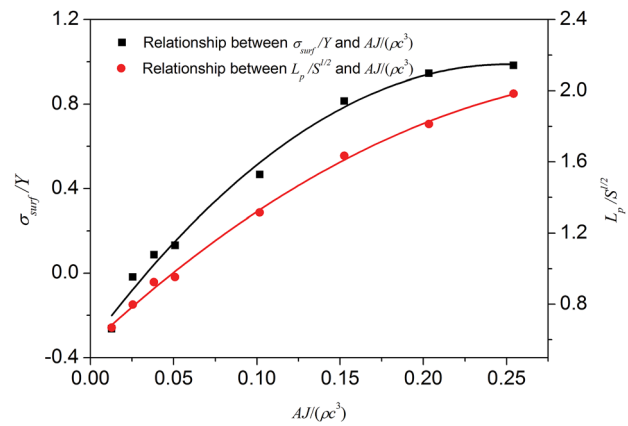

FIG. 10. Influence of laser power density on shock effects, in which the dimensionless thickness of confined overlay and the dimensionless laser duration are fixed as 0.1 and 0.1066, respectively, and the dimensionless laser power density ranges from 0.0125 to 0.25. The other dimensionless parameters are kept constant as given in Table II.

stress and plastically affected depth increase with increasing laser power density. While the laser power density exceeds 0.033, the surface residual stress will change from compressive stress to tensile stress, which is ascribed to the excessive shock pressure just as predicted theoretically by Ballard.[14] In addition, the relationship between the laser power density and surface residual stress and plastically affected depth can be fitted by quadratic functions with high correlations of $R^2 = 0.988$ and $R^2 = 0.997$, respectively. Fabbro *et al.*[3] deduced that the peak shock pressure p is proportional to square root of the laser power density $I^{1/2}$ by using a physical model. From this point, the shock effects approximately have a linear relationship with peak shock pressure, which agrees with the analysis of Ballard,[14] while the peak shock pressure is relatively much higher than the Hugoniot elastic limit (HEL) of metallic target.

V. CONCLUSIONS

Scaling approach to LSP has been analyzed using dimensional and finite element method. With considering bulk compressibility and inertial effect of confined overlay and metallic target, the coupling mechanism between plasma expansion and dynamic deformation of the confined overlay and the metallic target is implemented. The main conclusions are as follows:

1. Geometrical scaling law for laser shock effects, which is crucial in LSP experiments to obtain an optimized parameter window, is deduced by dimensional analysis and validated by numerical simulation.
2. The influence of thickness of confined overlay and laser duration on the surface residual stress exhibits a competition mechanism between thickness of confined overlay and laser duration. While the thickness of confined overlay exceeds 0.7, the influence tendency of laser duration on surface residual stress changes to slightly reverse direction.
3. The plastically affected depth increases with increasing laser duration and is almost independent with the thickness of confined overlay when dimensionless laser duration is less than 0.12. However, when laser duration $\tau/(S^{1/2}/c)$ exceeds 0.12, the plastically affected depth decreases at the beginning and then increases with increasing thickness of confined overlay.
4. The surface residual stress and plastically affected depth increase quadratically with increasing laser power density.

ACKNOWLEDGMENTS

The authors would like to thank the National Natural Science Foundation of China (10972228 and 11002150) and Basic Research Equipment Project of Chinese Academy of Sciences (YZ200930) for financial support.

[1]C. S. Montross, T. Wei, L. Ye, G. Clark, and Y.-W. Mai, Int. J. Fatigue **24**(10), 1021–1036 (2002).
[2]P. Peyre and R. Fabbro, Opt. Quantum Electron. **27**(12), 1213–1229 (1995).
[3]R. Fabbro, J. Fournier, P. Ballard, D. Devaux, and J. Virmont, J. Appl. Phys. **68**, 775–784 (1990).
[4]J. Lu, K. Luo, A. Feng, J. Zhong, G. Sun, L. Zhang, and X. Qian, Zhongguo Jiguang (Chin. J. Lasers) **37**(10), 2662–2666 (2010).
[5]A. H. Clauer, *Surface Performance of Titanium*, edited by J. K. Gregory *et al*. (TMS Warrendale, PA, 1996), pp. 217–230.
[6]A. H. Clauer and D. F. Lahrman, Key Eng. Mater. **197**, 121–144 (2001).
[7]B. Fairand and A. Clauer, Proc. SPIE **0086**, 112–119 (1976).
[8]B. Fairand, B. Wilcox, W. Gallagher, and D. Williams, J. Appl. Phys. **43**, 3893–3895 (1972).
[9]K. Y. Luo, J. Z. Lu, Y. K. Zhang, J. Z. Zhou, L. F. Zhang, F. Z. Dai, L. Zhang, J. W. Zhong, and C. Y. Cui, Mater. Sci. Eng., A **528**(13–14), 4783–4788 (2011).
[10]R. Fabbro, P. Peyre, L. Berthe, and X. Scherpereel, J. Laser Appl. **10**, 265–280 (1998).
[11]X. Hong, S. B. Wang, D. H. Guo, H. X. Wu, J. Wang, Y. S. Dai, X. P. Xia, and Y. N. Xie, Opt. Laser Eng. **29**(6), 447–455 (1998).
[12]X. Q. Wu, Z. P. Duan, H. W. Song, Y. P. Wei, X. Wang, and C. G. Huang, J. Appl. Phys. **110**, 053112 (2011).
[13]X. Q. Wu, C. G. Huang, X. Wang, and H. W. Song, Int. J. Impact Eng. **38**(5), 322–329 (2011).
[14]P. Ballard, Doctoral thesis, Ecole Polytechnique, France, 1991.
[15]P. Ballard, J. Fournier, R. Fabbro, and J. Frelat, J. Phys. IV **1**(C3), 3 (1991).
[16]B. X. Wu and Y. C. Shin, J. Manuf. Sci. Eng., Trans. ASME **129**(1), 117–125 (2007).
[17]A. H. Clauer, B. P. Fairand, and B. A. Wilcox, Metall. Mater. Trans. A **8**(12), 1871–1876 (1977).
[18]P. Forget, M. Jeandin, and A. Lyoret, J. Phys. IV **3**(C7), 7 (1993).
[19]J. Fournier, P. Ballard, P. Merrien, J. Barralis, L. Castex, and R. Fabbro, J. Phys. III **1**(9), 1467–1480 (1991).
[20]J. O'Keefe, C. Skeen, and C. York, J. Appl. Phys. **44**, 4622–4626 (1973).
[21]P. Peyre, L. Berthe, X. Scherpereel, and R. Fabbro, J. Mater. Sci. **33**(6), 1421–1429 (1998).
[22]P. Peyre, R. Fabbro, P. Merrien, and H. Lieurade, Mater. Sci. Eng.: A **210**(1), 102–113 (1996).
[23]M. Shepard, P. Smith, and M. Amer, J. Mater. Eng. Perform. **10**(6), 670–678 (2001).
[24]W. Herrmann, J. Appl. Phys. **40**(6), 2490 (1969).
[25]R. G. McQueen and S. P. Marsh, J. Geophys. Res. **71**(6), 1751, doi:10.1029/JZ071i006p01751 (1966).
[26]Q. M. Tan, *Dimensional Analysis: With Case Studies in Mechanics* (Springer-Verlag, Beijing, 2011).
[27]C. M. Cheng and B. M. Xie, Collected works of C. M. Cheng (Science Press, Beijing, 2004), pp.166–190.
[28]J. O. Hallquist, LS-DYNA3D theoretical manual (Livermore Software Technology Corporation, 1993).
[29]J. Batteh, J. Appl. Phys. **53**(11), 7537 (1982).
[30]G. Kanel, S. Razorenov, A. Utkin, H. He, F. Jing, and X. Jin, High Press. Res. **16**(1), 27–44 (1998).
[31]G. Johnson and W. Cook, *paper presented at the Proceedings of the 7th International Symposium on Ballistics, The Hague, Netherlands*, 1983.
[32]P. Peyre, X. Scherpereel, L. Berthe, and R. Fabbro, Surf. Eng. **14**(5), 377–380 (1998).
[33]B. Fairand and A. Clauer, AIP Conf. Proc. **50**, 27–42 (1979).
[34]N. Anderholm, Appl. Phys. Lett. **16**(3), 113–115 (1970).
[35]J. E. Masse and G. Barreau, Surf. Coat. Technol. **70**(2–3), 231–234 (1995).